Journal of Ceramic Processing Research. Vol. 23, No. 1, pp. 53~56 (2022)
(Received 6 August 2021, Received in revised form 24 September 2021, Accepted 19 October 2021)
https://doi.org/10.36410/jcpr.2022.23.1.53

J O U R N A L O F
Ceramic Processing Research

Synthesis and Characterization of Calcium based perovskites for catalytic coal combustion

Xingze Li*
School of Materials Science and Engineering, Hubei Polytechnic University, Huangshi Hubei, 435003, China

Opportunities and clean solution to improve the productivity and steadiness of renewable energy equipment have been provided by perovskite oxide materials. Nanomaterials made from metal oxides have the forefront of current technology and science research efforts due to their chemical, compositions, physical, properties and unique forms. Neuroscientists used a thermal treatment process to make $Ca_{0.8}$ $La_{0.2}Ti_{0.8}O_3$ perovskites. The XRD analysis revealed a cubic crystal symmetrical single-stage perovskite. The morphology of the particles was studied using scanning and SEM optical microscopy. The electronic conductivity of dopant $CaTiO_3$ was evaluated using impedance spectroscopy methods. This study's conductivity value suggests that this type of material could be useful as an electrode component in SOFCs.

Key words: Oxide materials, Perovskites, Hydrothermal method, XRD, Conductivity.

Introduction

Renewable energy and environmentally friendly technologies must be prioritised as we enter a new era. Energy is among the most important necessities for the existence of a self-sustaining international economy, and clean energy is a worldwide technical statement. For quite some time, scientists and technologists have been researching various aspects of energy issues. Advanced ways have been created to replace finite carbon fuels with more ecologically sustainable alternatives. The most popular resource is green resources. When an immediate supply of energy is required, renewables are site-specific, erratic, and unstable. Fuel cells, batteries, solar cells, and hydrogen generation are all examples of energy storage and conversion systems that have been created to minimise carbon output. Material research and development for energy applications has been hampered by Surface oxidation reaction benefit from particular compositions, topologies, and morphology and microstructure that help with active materials and electronic flaws. Rapid ion mobility in oxide materials is currently attracting researchers' attention. At high temperatures, solid solutions with electrolytes are used at room temperature are used in semiconductor devices reactors, hyper capacitors, electroactive displays, and electrolyte solar cell detectors are all examples of electrochemical solid-state devices. Oxygen detectors, reactive distillation membrane, and some other electronics all use oxide ion conductors. Over the last few decades, the properties of ionic conductivity compounds with diverse structures (ZnO, Fluorites, and Apatites) have been widely researched. Acceptor or donor doping was later thought to be a successful method for modifying defect concentrations in oxide materials and achieving electrical or transport capabilities that are desired Soon after emphasis shifted to having two cations of different valence states yet equal sizes, to ternary or larger oxides. To improve the desired characteristic, further doping was added to these oxides. At high temperatures, electrolytic and electronically oxides conductivity are key quality features for better converts energy to electricity in the present substitution technique. According to with polycrystalline oxides structure, certain Constituting ions are transported from one site to the next in the crystal until the electricity required to overcome barriers to step through one site to the next is negligible. The ($CaTiO_3$) orthorhombic and stability even at high temperatures. When a smaller radius negative electrode and a large oxide ion are joined, a cubic near-crystalline nature of O_2 ions with intervening metal ions is created. Perovskite is a crystal structure formed by partially replacing oxygen with cation and having the chemical formula ABX3. One of the most important ferroelectric perovskites is $CaTiO_3$. due to its dielectric properties and structural transformation flexibility [10-12]. It's been widely used in electrical products as a dopant and for radioactive waste.

$CaTiO_3$ is a great high charged particle conductivity, according to the literature. Nanoscale oxide compounds are now providing new ways to improve the efficiency and accuracy of sustainable energy generation and storage devices. Due to their unique shapes, physical properties, compositions, chemical and magnetic nano-

*Corresponding author:
Tel : +027-59750086
Fax: +027-59750085
E-mail: xingzeli5@163.com

particles are now at the forefront of current scientific research in all fields of innovation and science [9]. Reducing the overall temperature range of SOFCs from high towards mild temperatures have recently received a lot of interest due to benefits such as cheaper synthesizing and operational costs, adaptable cell hardware, and exergonic operation. In light of these findings, we investigated the effect of trace amounts of La in $CaTiO_3$ on its conductivity. A hydrothermal approach was used to investigate the functional and electrical properties of $Ca_{0.8}$ $La_{0.2}Ti_{0.8}O_3$ in this characteristic.

Summary of Materials and Techniques

$Ca_{0.8}$ $La_{0.2}Ti_{0.8}O_3$ of analytical quality was made with $Ca(NO_3)_2$, $La(NO_3)_{3.6}H_2O$, and $C_{12}H_{28}O_4Ti$, NaOH. Sigma-Aldrich provided all of these reagents, which were all 99.9% pure. Standard hydrothermal procedures were used to make these minerals (CH). To make a clear homogenous solution, the appropriate molar counterparts of the vital precursors have been dissolved in distilled water. To acidify the solution, a 10 M NaOH liquid is added until the pH reaches 11. After adding the NaOH, a white precipitate formed, which was subsequently autoclaved for 200 min. Once the process is complete, the catalyst is purified out, rinsed and ethyl alcohol, and left to dry, obtaining a pure white powder substance. Without first being calcined for 6 h at 700 ºC, the powder has been warmed to 120 ºC in a drying oven to evaporate water. In a shaking incubator, the carbonised samples were ground before even being difficult perpendicularly into 1.6 mm thick and 10 mm shaped cylinder pellets that used a pressure hydrostatic press set at 180 kg/cm^2. Before being employed for further characterisation and impedance analysis, the pellets were sintered for 6 h at 1,000 degrees Celsius using a standard sintering technique. The phase research was conducted out using an X-ray powder spectra were recorded (X'pert Pro, PAN alytical) equipped with Ni filtering CuK radioactivity and the capacity to switch the temp in 0.016º increments from 10 to 90º. A transmission electron microscope was used to examine the surface morphological characteristics of carbonised and sintered pellets (JEOL JSM-5600LV). Transmission electron microscopy was used to examine the morphological and compositional structure of the crystal structure using a JEOL JEM 2100 HRTEM (TEM).

Results and Discussions

Structure and X-ray diffraction analysis

The cubic perovskite structure is responsible for all diffraction peaks, according to JCPDS 752-100 at 1,000 ºC for 6 h is shown in Fig. 1. There were no other peaks, indicating there was no pure phase substance present as well as verifying the La doped roles in the $CaTiO_3$ structure. The perovskite's crystalline structure

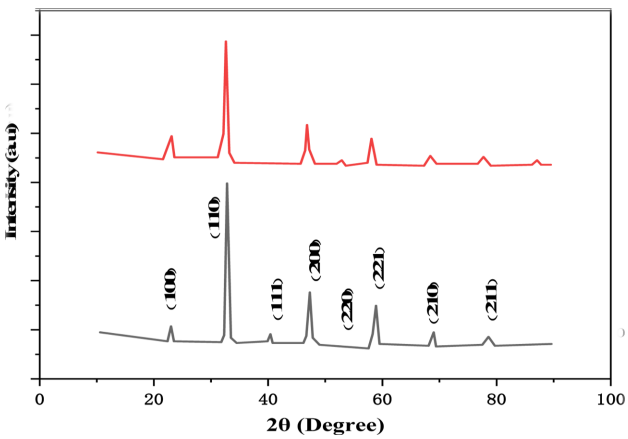

Fig. 1. $Ca_{0.8}$ $La_{0.2}TiO_{3-\delta}$ powder XRD pattern.

is further confirmed by the distinct powerful peaks.

Electron microscopy research

SEM observations

SEM was used to investigate sintered pellets and calcined powders. Fig. 2 shows Sintered, thermally engraved polished surfaces micrographed. The calcined particles have a minor agglomeration. According to micrographs, the pellets have definite grain boundaries and have been fully sintered. Micrographs show decreased porosity, indicating that the sintered pellets have become denser.

High-Resolution Transmission Electron Microscopy (HRTEM)

The morphology of calcined powder is shown in Fig. 2(b). According to microscope analysis, the calcined powder particles exhibit an uneven form. The particles are around 10 nm in size, according to the micrographs. The SAED (selected area for electron diffraction) is shown in the insets. Because of the nanosize of the particles, SAED forms ring patterns. Fig. 2 shows an HRTEM image created by smashing sintered pellets made from powder particles (d). All of the sintered pellets have a flaky morphology when seen at a lower magnification. Single crystalline flakes can be seen in SAED spot patterns.

Studies on impedance spectroscopy

The electronic behaviour of the produced samples were determined using impedance analysis. In parallel R-C cells, a materials AC impedance reaction occurs. The single impedance Z of the R-C cell is determined by

$$Z = Z' + jZ'' \quad (1)$$

Z' stands for the real component of Z, while Z'' stands for the imagined part. In an air environment with a room temperature of 30-750 ºC, conductivity analysis was performed to examine the conductivity of

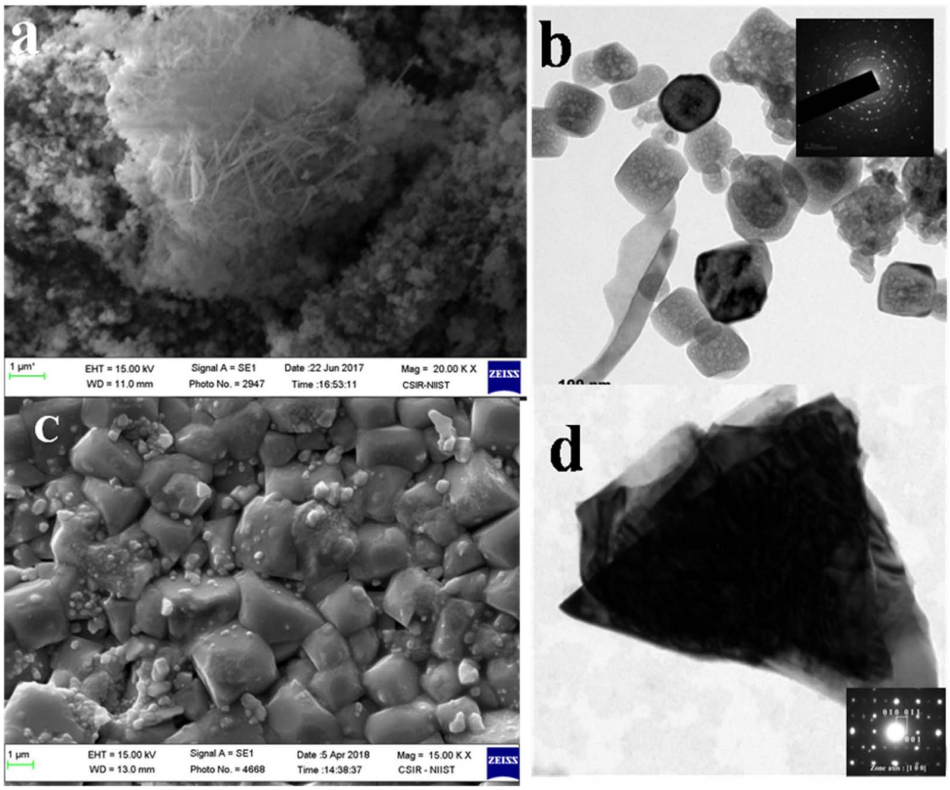

Fig. 2. SEM and HRTEM micrographs of calcined powders, sintered pellets.

the specimens across a broad frequency band (50 Hz to 10 MHz). In Nyquist diagrams, the imaginary and appropriate impedance sections are represented by a semi-circle series (Cole-Cole plot). Fig. 3 shows the Cole-Cole plot. The quasi from of the curve on the Z can be used to calculate the resistance (x-axis). As the temperature increases, the radius of both the semicircle reduces, indicating a loss of strength.

Because the relaxation durations correlating to intergranular are the same for some materials, the impedance information cannot be split into more than just semicircle. A similar trend had previously been observed in doped cerium oxide [14]. The following equation was used to compute the combined conductivity:

$$\rho = \frac{1}{RA} \text{ S/cm} \quad (2)$$

The sampling electrode area and showing information are represented by l and A, correspondingly. Total conductivity in an air atmosphere between 600 to 750 ºC varies from 10^{-3} to 10^{-4} Scm^{-1}. Total permeability (log) vs. temperature dependence (1000/T) is depicted in Fig. 4. Heat transfer rate increases in a nearly linear way, per the Arrhenius.

$$\sigma = \sigma_0 \exp(-E_a / K_B T) \quad (3)$$

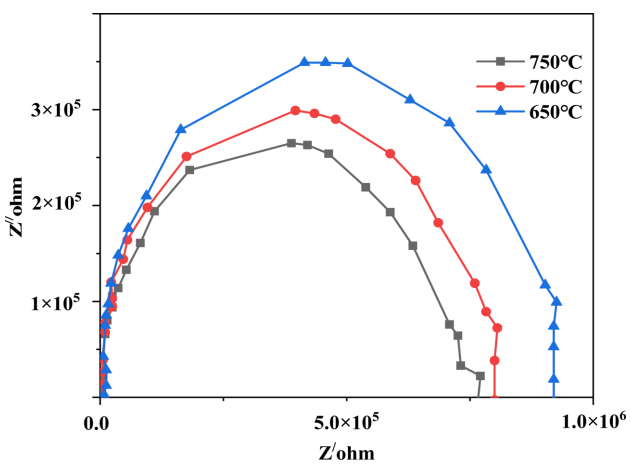

Fig. 3. At three different temperatures, the Cole-Cole plots.

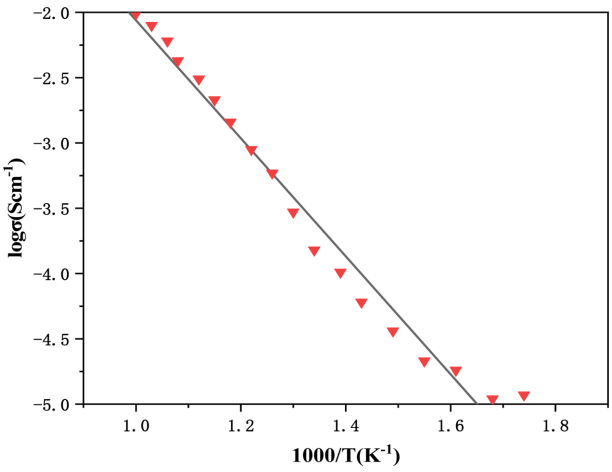

Fig. 4. Plot of log conductivity with respect to inverse temperature.

The activation energy is represented by E_a, T represents the absolute temperature, 0 represents k, the pre-exponential factor represents Boltzmann's constant. For $Ca_{0.8}$ $La_{0.2}Ti_{0.8}$ $Ta_{0.2}O_3^-$ for $Ca_{0.8}$ $La_{0.2}Ti_{0.8}$ Ta Based on the Arrhenius figure, the activation energy is determined to be 0.85 eV. This shows that the material could be used as an electrolyte in SOFCs with temperatures below 750 °C.

Conclusion

$Ca_{0.8}$ $La_{0.2}Ti_{0.8}O_3$ is synthesised by a hydrothermal process. After doping lanthanum into the parent molecule, the crystal lattice revealed a cubic fluorite framework, and structural stability was maintained. The morphology of sintered pellets as seen under a scanning electron microscope shows a decrease in porosity. Conductivity improves as temperature rises, according to impedance analysis.

References

1. S. Chandra, in “Superionic solids : principles and applications” (Amsterdam, 1981) p.15.
2. P.G. Bruce, in “Solid State Electrochemistry” (Cambridge University Press, 1995) p.165.
3. B.C. H Steele, J. Power Sources 49 (1994) 1-14.
4. A.D. Logan and M. Shelef, J. Mater. Res. 9 (1994) 468-475.
5. P. Knauth and H.L. Tuller J. Eur. Ceram. Soc. 19 (1999) 831-836.
6. N. Bonanos, K.S. Knight, and B. Ellis, Solid State Ion. 79 (1995) 161-170.
7. K.R. Kendall, C. Navas, J.K. Tomas, H.C. Zur Loye, Solid State Ion. 82 (1995) 215-223.
8. D. Rajendran, K.R. Nair, P.P. Rao, KS. Sibi, P. Koshy, and V.K. Vaidyan, Mater. Lett. 62 (2008) 623-628.
9. B. Madhavan and A. Ashok, J. Solgel Sci. Technol. 73 (2015) 1-8.
10. E. Cockayne and B.P. Burton, Phys. Rev. B 62 (2000) 3735.
11. T. Nakamura, P.H. Sun, Y.J. Shan, Y. Inaguma, M. Itoh, I.S Kim, J. H Sohn, M. Ikeda, T itamura, H. Konagaya 196 (1997) 205-209.
12. J. Maier, Solid State Ion. 154 (2002) 291-301.
13. N. Q. Minh, J. Am. Ceram. Soc. 76 (1993) 563-588.
14. C. Sun, H. Li, L. Chen, Energy Environ. Sci. 5 (2012) 8475-8505.